UNIVERSITY OF CALIFORNIA, SAN DIEGO

Progress Toward Analytic Predictions of Supersonic Hydrocarbon-Air Combustion: Computation of Ignition Times and Supersonic Mixing Layers

A thesis submitted in partial satisfaction
of the requirements for the degree of Master of Science

in

Engineering Sciences (Mechanical Engineering)

by

Scott Michael Sexton

Committee in charge:

Professor Antonio Sánchez, Chair
Professor Kalyanasundaram Seshadri
Professor Forman Williams

2017

The Thesis of Scott Michael Sexton is approved, and it is acceptable in quality and form for publication on microfilm and electronically:

Chair

University of California, San Diego

2017

DEDICATION

To my dad, who has demonstrated the best way a man should live, and has guided and supported me with an incomprehensible level of selflessness. To my mom, the rock holding me steady through the best and worst of times, with a love that I cannot begin to understand. To my sister, whose admiration is my most tremendous inspiration to brave the unfamiliar. To my uncle, who has challenged me, taught me, advised me, and shown what is possible through higher education.

Table of Contents

List of Figures

List of Tables

ABSTRACT OF THE THESIS

Progress Toward Analytic Predictions of Supersonic Hydrocarbon-Air Combustion: Computation of Ignition Times and Supersonic Mixing Layers

by

Scott Michael Sexton

Master of Science in Engineering Sciences (Mechanical Engineering)

University of California, San Diego, 2017

Professor Antonio Sánchez, Chair

Combustion in scramjet engines is faced with the limitation of brief residence time in the combustion chamber, requiring fuel and preheated air streams to mix and ignite in a matter of milliseconds. Accurate predictions of autoignition times are needed to design reliable supersonic combustion chambers. Most efforts in estimating non-premixed autoignition times have been devoted to hydrogen-air mixtures. The present work addresses hydrocarbon-air combustion, which is of interest for future scramjet engines.

Computation of ignition in supersonic flows requires adequate characterization of ignition

chemistry and description of the flow, both of which are derived in this work. In particular, we have shown that activation energy asymptotics combined with a previously derived reduced chemical kinetic mechanism provides analytic predictions of autoignition times in homogeneous systems. Results are compared with data from shock tube experiments, and previous expressions which employ a fuel depletion criterion.

Ignition in scramjet engines has a strong dependence on temperature, which is found by perturbing the chemically frozen mixing layer solution. The frozen solution is obtained here, accounting for effects of viscous dissipation between the fuel and air streams. We investigate variations of thermodynamic and transport properties, and compare these to simplified mixing layers which neglect these variations. Numerically integrating the mixing layer problem reveals a nonmonotonic temperature profile, with a peak occurring inside the shear layer for sufficiently high Mach numbers.

These results will be essential in computation of ignition distances in supersonic combustion chambers.

1 Introduction

Supersonic combustion ramjet engines (or scramjets) are unique in that combustion occurs in the combustion chamber at supersonic velocities. The interaction of the supersonic fuel and air heats the mixture through viscous dissipation, raising the mixture temperature to the autoignition point. This effect means an ignitor is not required in the combustion chamber, drastically simplifying design of the engine. In order to use this effect efficiently and safely, designers must know where in the engine combustion occurs. Because combustion occurs at supersonic velocities, residence times inside the chamber are on the order of milliseconds. Accurate knowledge of heating and the ignition mechanism are required to characterize induction length. These phenomena are explored here for hydrocarbon fuels, which are of interest for future scramjet engines.

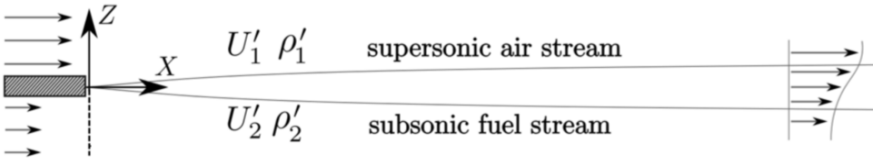

Figure 1: Subsonic-supersonic fuel-air mixing layer [1].

The interaction of fuel and air within the supersonic mixing layer may be characterized as homogenous combustion, which has been studied experimentally, analytically, and numerically for n-alkanes. Peters [2] has presented a simplified chemical kinetic mechanism for n-heptane ignition, which is adjusted further by Saxena and Williams [3]. Saxena *et al.* propose an analytic expression to describe time to autoignition using fuel depletion as the criterion for ignition. Using the updated chemical kinetics [4], Saxena's expression falls out of agreement with experimental shock tube data [5]- [8]. The present work seeks to improve on Saxena's expression by including the influence of heat released during decomposition of the parent fuel and intermediate hydrocarbons, letting thermal runaway characterize autoignition time.

This combustion occurs in a mixing layer that forms between a subsonic fuel and the supersonic air stream into which it is injected. Large velocity differences result in large temperature

rises by viscous heating, which has been investigated previously [9]- [11]. The mixing layer may be simplified by calling it chemically frozen, neglecting any effects of chemical reaction. Properties of this frozen free shear layer may be found numerically by solving the momentum, energy, and mass conservation equations. The solution proves quite sensitive to transport and thermodynamic properties, where significant error occurs if not accounted for correctly or ignored.

2 Reduced Chemistry for Homogenous Hydrocarbon Ignition

Combustion modeling of alkanes such as n-heptane requires 56 reaction steps to show good agreement of ignition times with shock tube experiments through low, intermediate, and high temperature ignition [2]. While 56 steps is a drastic reduction of the complete forward and backward combustion mechanism, it is still not practical for deriving analytical expressions or numerical methods to compute time to ignition of normal aklanes.

2.1 Reduced Chemistry per Peters *et al.*

Peters *et al.* [1] provide a method for reducing these 56 steps to just four reaction steps, primarily by recognizing that many radicals approach steady state for most of induction in the high temperature regime, and that many of the 56 reactions occur so fast that they need not be included in the reduced chemistry. Once these 4 steps were laid out, an analytic expression for the ignition time may be derived. In particular, they note that at high temperatures, ketohydroperoxide (HOOCH2OCHO) approaches steady state, and a steady rise in hydrogen peroxide $[\mathrm{H_2O_2}]$ directly influences concentration of hydroperoxyl $\mathrm{HO_2}$. These assumptions lay groundwork for Saxena's formulation of an ignition time expression based on fuel depletion [3], and simplification to a single equation describing the high temperature ignition region.

2.2 Reduced Chemistry per Saxena *et al.*

Another method of simplification is put forth by Saxena *et al.* [3] by post processing re-

sults from a detailed combustion simulation of propane using the San Diego Mechanism [12] in FlameMaster [13], a computer program for zero dimensional combustion and one dimensional laminar flames. The rate of $\mathrm{C_mH_n}$ consumption is equal to the total rate of production of all isomers $\mathrm{C_mH_{n-1}}$, which is highly reactive. The primary consumers of fuel are H and OH radicals, followed by $\mathrm{HO_2}$, then the much slower O radicals, which were omitted from the reduced chemistry. H and OH concentrations are seen to remain at approximately steady state (<1% variation) for the first $\sim 70\ \mu\mathrm{s}$ of induction. $\mathrm{HO_2}$ variation remains below 10% for the second half of induction ($40\ \mu\mathrm{s} - 100\ \mu\mathrm{s}$). In light of these concentrations, these radicals may be assumed to maintain steady state until ignition time $\mathrm{t_i}$.

Since the primary H consumption step is $\mathrm{C}_m\mathrm{H}_n + \mathrm{H} \xrightarrow{1} \mathrm{C}_m\mathrm{H}_{n-1} + \mathrm{H_2}$ (table 1, step 1), and the primary source of H is step 5, $\mathrm{OH} + \mathrm{H_2} \xrightarrow{5} \mathrm{H_2O} + \mathrm{H}$, the reaction rates ω_1 and ω_5 are approximately equal. Similar logic may be applied to the main sink and source of OH (steps 2 and 6), $\mathrm{C}_m\mathrm{H}_n + \mathrm{OH} \xrightarrow{2} \mathrm{C}_m\mathrm{H}_{n-1} + \mathrm{H_2O}$ and $\mathrm{H_2O_2} + (\mathrm{M}) \xrightarrow{6} 2\,\mathrm{OH} + (\mathrm{M})$, so that ω_2 equals rate ω_6. This, then, requires the net production of OH must equal net consumption of OH, meaning ω_6 equals one half of $(\omega_2 + \omega_5)$ Since ω_1 equals ω_5, the reaction rate ω_6 equals one half$(\omega_1 + \omega_2)$, where reactions 1 and 2 are two of three reactions attacking the parent fuel $\mathrm{C_mH_n}$. Therefore, the net rate of consumption of fuel is $\omega_{\mathrm{C_mH_n}}$ is $2\omega_6 + \omega_3$.

Table 1: Reduced chemical kinetic mechanism [3].

1	$\mathrm{C}_m\mathrm{H}_n + \mathrm{H}$	$\longrightarrow$	$\mathrm{C}_m\mathrm{H}_{n-1} + \mathrm{H_2}$
2	$\mathrm{C}_m\mathrm{H}_n + \mathrm{OH}$	$\longrightarrow$	$\mathrm{C}_m\mathrm{H}_{n-1} + \mathrm{H_2O}$
3	$\mathrm{C}_m\mathrm{H}_n + \mathrm{HO_2}$	$\longrightarrow$	$\mathrm{C}_m\mathrm{H}_{n-1} + \mathrm{H_2O_2}$
4	$\mathrm{C}_m\mathrm{H}_{n-1} + \mathrm{O_2}$	$\longrightarrow$	$\mathrm{HO_2} + \mathrm{P}$
5	$\mathrm{OH} + \mathrm{H_2}$	$\longrightarrow$	$\mathrm{H_2O} + \mathrm{H}$
6	$\mathrm{H_2O_2} + (\mathrm{M})$	$\longrightarrow$	$2\,\mathrm{OH} + (\mathrm{M})$
7	$2\,\mathrm{HO_2}$	$\longrightarrow$	$\mathrm{H_2O_2} + \mathrm{O_2}$

Production of $\mathrm{HO_2}$ may be approximated by use of the rapid alkyl decomposition step, $\mathrm{C}_m\mathrm{H}_{n-1} + \mathrm{O_2} \xrightarrow{4} \mathrm{HO_2} + \mathrm{P}$, where P represents smaller, more stable products such as CO, $\mathrm{CO_2}$, and $\mathrm{H_2O}$. The intermediates formed by this decomposition are either volatile enough to rapidly decompose into smaller products, or stable enough that they interact with $\mathrm{O_2}$ to form $\mathrm{HO_2}$. This

implies the net rate of production of HO_2 is the rate of production of C_mH_{n-1} (which is also the rate of consumption of the parent fuel $\omega_{C_mH_n}$) minus rate ω_3. H_2O_2 is also consumed through the step $2\,HO_2 \xrightarrow{7} H_2O_2 + O_2$, leading to rate ω_7 approximately equalling one half of $\omega_{C_mH_n} - \omega_3$. Since $\omega_{C_mH_n} = 2\omega_6 + \omega_3$, substituting for $\omega_{C_mH_n}$ yields the somewhat startling, yet convenient fact that ω_7 equals ω_6. This convenience allows for an equation relating hydroperoxyl concentration:

$$k_7[HO_2]^2 = k6[M][H_2O_2] \tag{1}$$

which, rearranging, gives:

$$[HO_2] = \sqrt{\frac{k_6}{k_7}[M][H_2O_2]} \tag{2}$$

Combining steps 3 and 4 (table 1) gives an overall reaction step I:

$$C_mH_n + O_2 \xrightarrow{I} H_2O_2 + P \tag{3}$$

where P represents the completely decomposed products of perfect combustion, CO, CO_2, and H_2O. Reaction I is limited by rate ω_3:

$$\omega_3 = k_3[C_mH_n]\sqrt{\frac{k_6}{k_7}[M][H_2O_2]} \tag{4}$$

Combining steps 2, 4, 6, and 7 (table 1) eliminates dependence on OH and HO_2, and gives the second overall step II:

$$2\,C_mH_n + O_2 \xrightarrow{II} 2\,H_2O + 2\,P \tag{5}$$

which is limited by reaction rate ω_6:

$$\omega_6 = k_6[M][H_2O_2] \tag{6}$$

When compared with the 56 step chemistry, the intermediate reduced 30 step chemistry put forth by Peters [2] shows error on the order of scatter shown in experimental results, and the 4 step reduced chemistry shows error less than 10%. Similar error is found with the reduced ignition time formula derived by Saxena [3], but increases slightly when the most recent San Diego Mechanism [4] is applied to Arrhenius reaction coefficients.

2.3 Reaction Path Sensitivity

Saxena *et al.* [3] performed a sensitivity analysis on the reaction path of the full 358 steps that define propane combustion. They found, unsurprisingly, that the chain initiation step $C_3H_8 + M \longrightarrow CH_3 + C_2H_5 + M$ had the largest influence (highest sensitivity) on the reaction. Reaction step 6 (table 1) was found to be the 16th most sensitive step, while reaction steps 3 (isomers of C_mH_{n-1}, $1-C_3H_7$ and $2-C_3H_7$) were 54th and 65th, and step 7 was 157th sensitive of 358 steps. Interestingly, agreements within 10% are found using relatively insensitive reactions to govern the ignition time criteria. This confirms the steady state approximations made earlier are justified under these conditions, and their validity need not be questioned further.

3 Derivation of the Ignition Time Formula

In attempts by Saxena, Peters, and Williams [3] to characterize the time to autoignition of n-alkanes, analytic expressions have been proposed which take into account pressure, temperature, fuel concentration, and Arrhenius reaction rate coefficients of fuel-air mixtures. For hydrogen combustion, Boivin, Sanchez, and Williams [14] have presented a method to incorporate heats of reaction into the ignition time expression, but the author is unaware of a similar analytic expression supporting ignition of n-alkanes.

What follows is a presentation of the ignition time expression derived by Saxena *et al.* [3], and an effort to improve upon their expression by accounting for the heats of reaction of the reduced reactions I and II (Equations 3 and 5) akin to the method put forth by Boivin *et al.* [14]. The hope is

this method will provide a higher order of accuracy when applied to autoignition of the supersonic mixing layer by including the energy exchanged during breakdown of aklenes and alkyl radicals, as well as the formation of smaller products such as CO, CO_2, and H_2O.

3.1 Ignition Time Defined by Fuel Depletion per Saxena *et al.*

Peters [2] and Saxena [3] propose that a viable criterion for ignition time is complete depletion of the parent fuel. This criterion suits the problem well because fuel is depleted at a finite time t_i, which may be computed by integrating the differential fuel concentration with respect to time, $d[C_mH_n]/dt$. Also, as found in FlameMaster simulations by Pitsch [13], the reaction exhibits a rapid and drastic increase in temperature at the point where fuel concentration $[C_mH_n]$ approaches the same order of radical concentrations, and temperature nearly doubles within the final $15\ \mu s$ of induction. In addition, the parent fuel molecules have a net termination effect, restricting chain branching reactions from occurring due to H, O, and OH radicals. The reaction rates of H and O radicals reacting with the parent fuel C_mH_n are at minimum on the order of the reaction rates of the fuel's decomposed intermediate hydrocarbons.

Using the formulation of the overall reduced chemistry in Section 2.2, Saxena [3] puts forth the rates of fuel and hydrogen peroxide consumptions:

$$\frac{d[C_mH_n]}{dt} = -k_3[C_mH_n]\sqrt{\frac{k_6}{k_7}[M][H_2O_2]} - 2k_6[M][H_2O_2] \tag{7}$$

$$\frac{d[H_2O_2]}{dt} = k_3[C_mH_n]\sqrt{\frac{k_6}{k_7}[M][H_2O_2]} \tag{8}$$

and defines a dimensionless time τ, assuming the third body concentration [M] remains constant:

$$\tau = t\left(\frac{2k_6^2k_3^2}{k_7}[M]^2[C_mH_n]_0\right)^{1/3} \tag{9}$$

By use of

$$\mathrm{x} = \frac{[\mathrm{C_mH_n}]}{[\mathrm{C_mH_n}]_0} \tag{10}$$

$$\mathrm{y} = \frac{[\mathrm{H_2O_2}]}{[\mathrm{C_mH_n}]_0} \left(\frac{4\mathrm{k_6k_7[M]}}{\mathrm{k_3^2}[\mathrm{C_mH_n}]_0} \right)^{1/3} \tag{11}$$

$$\mathrm{a} = \left(\frac{\mathrm{k_3^2}[\mathrm{C_mH_n}]_0}{4\mathrm{k_6k_7[M]}} \right)^{1/3} \tag{12}$$

equations for the evolution of fuel and hydrogen peroxide concentration (7 and 8) become:

$$\frac{\mathrm{dx}}{\mathrm{d}\tau} = -\mathrm{y} - \mathrm{ax}\sqrt{\mathrm{y}} \tag{13}$$

$$\frac{\mathrm{dy}}{\mathrm{d}\tau} = \mathrm{x}\sqrt{\mathrm{y}} \tag{14}$$

with initial conditions $\mathrm{x} = 1$ and $\mathrm{y} = 0$ at $\tau = 0$. Introducing $\mathrm{z} = \sqrt{\mathrm{y}}$, the above reduces to:

$$\frac{\mathrm{dx}}{\mathrm{d}\tau} = -\mathrm{z}^2 - \mathrm{axz} \tag{15}$$

$$\frac{\mathrm{dy}}{\mathrm{d}\tau} = \frac{\mathrm{x}}{2} \tag{16}$$

which leads to the second order, nonlinear differential equation:

$$\frac{\mathrm{d}^2\mathrm{z}}{\mathrm{d}\tau^2} + \mathrm{az}\frac{\mathrm{dz}}{\mathrm{d}\tau} + \frac{\mathrm{z}^2}{2} = 0 \tag{17}$$

This equation requires initial conditions at $\tau = 0$:

$$\frac{\mathrm{dz}}{\mathrm{d}\tau} = \frac{1}{2} \tag{18}$$

$$\mathrm{z} = 0 \tag{19}$$

Letting $\mathrm{u} = \mathrm{dz}/\mathrm{d}\tau$, Equations 17 and 18 may be written as:

$$\frac{\mathrm{d}(\mathrm{u}^2)}{\mathrm{dz}} = -\mathrm{z}^2 \tag{20}$$

$$\mathrm{u} = \frac{1}{2} \tag{21}$$

at $\mathrm{z} = 0$. This system has the solution

$$u = \sqrt{\frac{1}{4} - \frac{\mathrm{z}^3}{3}} \tag{22}$$

Fuel is depleted when $\mathrm{x} = 0$, which corresponds to $\mathrm{u} = 0$, so the dimensionless induction time Equation 9 is found by using the substitution $\mathrm{v} = \mathrm{z}/(3/4)^{1/3}$ to numerically integrate:

$$\tau_\mathrm{i} = \int_0^{(3/4)^{1/3}} \mathrm{u}^{-1}\mathrm{dz} \tag{23}$$

$$= 6^{1/3} \int_0^1 (1 - \mathrm{v}^3)^{-1/2}\mathrm{dv} = 2.548 \tag{24}$$

which yields the time to autoignition:

$$\mathrm{t_i} = \left(8.27 \frac{\mathrm{k_7}}{\mathrm{k_6^2 k_3^2 [M]^2 [C_m H_n]_0}}\right)^{1/3} \tag{25}$$

This expression gives the time at which fuel is completely depleted. It accounts for initial temperature, pressure, and concentrations of the fuel-air mixture by including the third body concentration $[\mathrm{M}]$ and initial fuel concentration $[\mathrm{C_m H_n}]_0$, and uses the limiting reaction rate constants $\mathrm{k_3}$, $\mathrm{k_6}$, and $\mathrm{k_7}$. Approximations of the ignition time are plotted in Figures 3-7.

3.2 Ignition Time Defined by Thermal Runaway per Sexton and Sánchez

Omitted in the formulation put forth by Saxena *et al.*, P in reaction I (Equation 3) represents the products formed by complete decomposition of $\mathrm{C_m H_n}$ (subsequently $\mathrm{C_m H_{n-1}}$, along with all other intermediate hydrocarbons). Accounting for heats of reaction permits deriving an

energy balance equation for the reaction. Upon complete decomposition of $\mathrm{C_mH_n}$ and formation of $\mathrm{H_2O_2}$, heat is released, and the reaction exhibits thermal runaway, defined as a rapid increase in temperature of the mixture, a common criterion for defining ignition. For combustion of n-alkanes due to rapid decomposition of $\mathrm{C_mH_{n-1}}$ radicals, P becomes:

$$\mathrm{P} = \mathrm{mCO} + \frac{\mathrm{n}-2}{2}\mathrm{H_2O} \tag{26}$$

This decomposition is exothermic, and while $\mathrm{C_mH_{n-1}}$ does oxidize into $\mathrm{CO_2}$, its oxidation step is much slower than the formation of CO, so we exclude $\mathrm{CO_2}$ from the final products P.

Table 2: Enthalpies of formation of n-alkanes and their products [15].

Constituent	$\Delta \mathrm{H_f^o}$ (J/mol)
$\mathrm{C_3H_8}$	-104.7E3
$\mathrm{C_4H_{10}}$	-125.5E3
$\mathrm{C_5H_{12}}$	-146.9E3
$\mathrm{C_7H_{16}}$	-187.9E3
$\mathrm{C_{10}H_{22}}$	-249.4E3
$\mathrm{H_2O}$	-241.8E3
$\mathrm{H_2O_2}$	-187.8E3
CO	-110.5E3

Heats of reaction $\mathrm{q_I}$ and $\mathrm{q_{II}}$ (steps I and II) are determined from the enthalpies of formation of the hydrocarbon fuels, $\mathrm{H_2O_2}$, CO, and $\mathrm{H_2O}$. Values of $\mathrm{q_I}$ and $\mathrm{q_{II}}$ are calculated using values found in table 2 with the following:

$$\mathrm{q_I} = \mathrm{h_{fuel}} - \mathrm{h_{H_2O_2}} - \mathrm{mh_{CO}} - \frac{\mathrm{n}-2}{2}\mathrm{h_{H_2O}} \tag{27}$$

$$\mathrm{q_{II}} = 2\mathrm{h_{fuel}} - 2\mathrm{mh_{CO}} - \mathrm{nh_{H_2O}} \tag{28}$$

Similarly to the process put forth by Boivin, Sanchez, and Williams [7], including heats of

reaction in the energy conservation and hydrogen peroxide consumption equations gives:

$$\rho C_p \frac{dT}{dt} = q_I k_3 [C_m H_n] \sqrt{\frac{k_6}{k_7}[M][H_2O_2]} + q_{II} k_6 [M][H_2O_2] \tag{29}$$

$$\frac{d[H_2O_2]}{dt} = k_3 [C_m H_n] \sqrt{\frac{k_6}{k_7}[M][H_2O_2]} \tag{30}$$

which may be combined:

$$\rho C_p \frac{dT}{d[H_2O_2]} = q_I + \frac{q_{II} k_6}{\Psi}[M][H_2O_2]^{1/2} \tag{31}$$

Equations 29 and 30 are made dimensionless by use of the following:

$$q = \frac{q_{II}[M]}{\rho C_p T_0} \tag{32}$$

$$\Psi = k_3 [C_m H_n] \sqrt{\frac{k_6}{k_7}[M]} \tag{33}$$

$$[H_c] = (\frac{\Psi}{q \beta k_6})^{2/3} \tag{34}$$

$$t_c = (\Psi^2 q \beta k_6)^{-1/3} \tag{35}$$

$$\theta = \beta \frac{T - T_0}{T_0} \tag{36}$$

$$\Lambda = \frac{q_I}{q_{II}} \frac{1}{[M]} (\frac{\Psi^2}{k_6^2 q \beta})^{1/3} \tag{37}$$

$$\phi = \frac{[H_2O_2]}{[H_c]} \tag{38}$$

$$\tau = \frac{t}{t_c} \tag{39}$$

producing a first order differential equation:

$$\frac{d\theta}{d\phi} = \Lambda + \phi^{1/2} \tag{40}$$

Integrating to find θ with initial conditions $\theta = 0$ and $\phi = 0$, we have:

$$\begin{aligned}\theta &= \int_0^{\phi} \Lambda + \phi^{1/2} \\ &= \Lambda\phi + \frac{2}{3}\phi^{3/2}\end{aligned} \tag{41}$$

The expression for θ gives us the dimensionless temperature in terms of hydrogen peroxide concentration, which is estimated with a dimensionless hydrogen peroxide consumption equation, derived from 30. Inspecting reaction I (Equation 3) reveals as fuel is depleted, there is an increase in $[H_2O_2]$ (therefore, an increase in ϕ). From the expression relating θ and ϕ, as $\phi \to \infty$ (or $[H_2O_2] \to \infty$), dimensionless temperature θ also tends to infinity, which is the definition of thermal runaway, demonstrated in Figure 2. Therefore, nondimensionalizing Equation 30 and numerically integrating ϕ from $0 \to \infty$, τ is:

$$\frac{\mathrm{d}\phi}{\mathrm{d}\tau} = \mathrm{e}^{\theta}\phi^{1/2} \tag{42}$$

$$\tau = \int_0^{\infty} \mathrm{e}^{-\theta}\phi^{-1/2}\mathrm{d}\phi \approx 2.22 \tag{43}$$

Substituting τ into Equations 35 and 39 gives the induction time $\mathrm{t_i}$:

$$\mathrm{t_i} = 2.22(\Psi^2 \mathrm{q}\beta\mathrm{k_6})^{-1/3} \tag{44}$$

Comparisons of this improved ignition time expression are made to Saxena's fuel depletion formulation and experimental shock tube data in Section 3.3, which shed light on the benefits and limitations of using heats of reaction to compute thermal runaway as a criterion for ignition.

3.3 Comparisons of Ignition Time Formulae

Introducing heats of reaction to the ignition time formula allowed for use of thermal runaway to establish hydrocarbon ignition times. Temperature is easier to measure than species con-

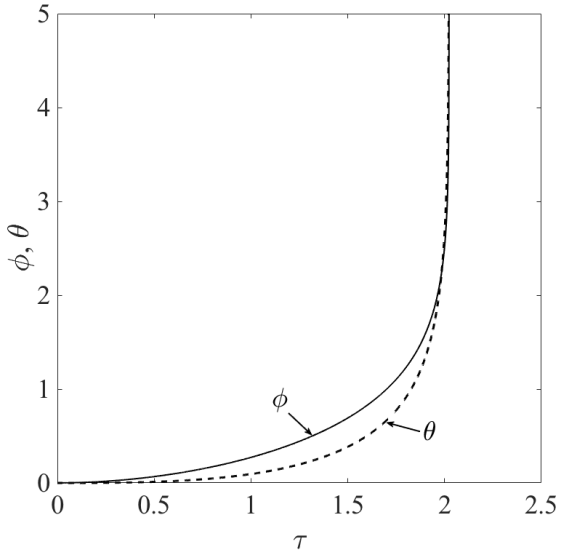

Figure 2: Thermal runaway demonstrated through dimensionless temperature θ and dimensionless H_2O_2 concentration ϕ as functions of dimensionless time τ.

centration, and facilitates better comparisons to experimental data. Decomposition into CO, CO_2, and H_2O is exothermic, releasing energy by breaking bonds in intermediate radicals. This increases the energy of the reaction, shortening the time to thermal runaway. When approximated with the updated reaction kinetics [4], the expression put forth by Saxena and Williams [3] overpredicts the time to ignition compared to experimental data, likely because they do not include the contribution of heat release from decomposition into CO and H_2O.

Another advantage is the thermal runaway criterion allows the reaction's strong temperature dependence to be introduced as a perturbation to the temperature profile of a chemically frozen mixing layer. This analysis was performed by Boivin *et. al.* [14] for hydrogen-air mixtures, and provides the induction length for the reaction in a supersonic combustion chamber. Future work may include this perturbation analysis, using the activation energy β as a perturbation to the temperature distribution established in Section 4.2.

Shock tube experiments characterize ignition times by measuring the time between the reflected shock and flame front passing a measurement point. Detection of the shock wave is possible with a pressure transducer, while detection of a flame front is possible by measuring

traces of intermediate species. If the reaction is sufficiently exothermic, a pressure measurement alone is sufficient to detect ignition. Errors in experimental ignition time of $\pm 10\%$ are common for such experiments.

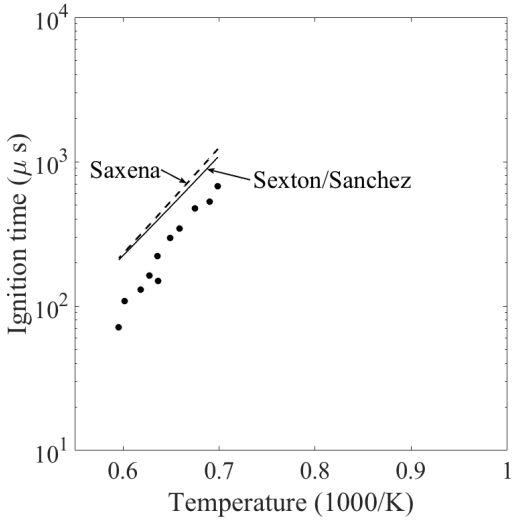

Figure 3: Comparison of experimental shock tube data [5] to analytic expressions for homogenous autoignition time of propane.

Improvements on the ignition time expression over the fuel depletion criterion are less pronounced for the propane (Figure 3) mixture tested here than for other mixtures, mostly due to the reduced influence of q on the temperature rise of the reaction. Experimental shock tube data used for comparisons of propane and n-decane from used relatively low compositions of fuel compared to the overall mixture, only 0.2% (albeit still stoichiometric), compared to 2-2.5% for other fuels. This causes the net heat addition from q in Equation 44 to be reduced by ~ 10 times, a reduction in $10^{1/3} \approx 2.15$ times its influence on ignition time. Propane's small size and fewer number of bonds have a secondary effect, releasing less heat by intermediate radical decomposition, further diminishing the influence of q.

N-butane sees an underprediction of time to autoignition on the order of Saxena's overprediction (Figure 4). This, in part, is due to the high pressure of the mixture, about 2 times higher than other fuels tested. High pressures accelerate the reaction through the term Ψ^2, shortening time to ignition similarly to how fuel concentration affected propane combustion in Figure 3.

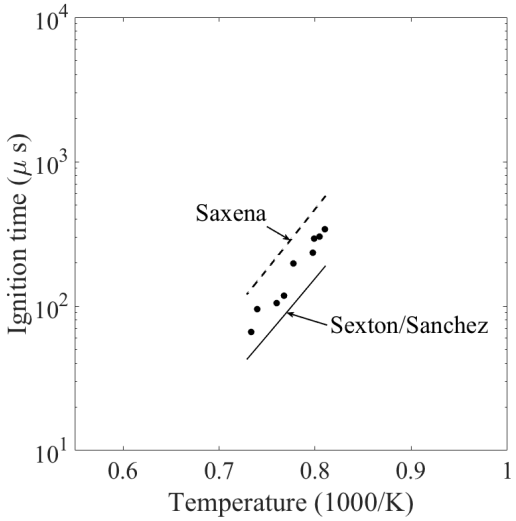

Figure 4: Comparison of experimental shock tube data [6] to analytic expressions for homogenous autoignition time of n-butane.

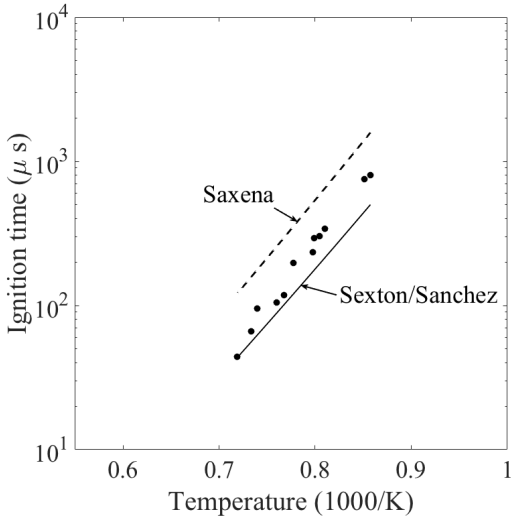

Figure 5: Comparison of experimental shock tube data [6] to analytic expressions for homogenous autoignition time of n-pentane.

The thermal runaway ignition time expression for estimating n-pentane ignition time shows very good improvement over Saxena's expression (Figure 5), due in part to its modest pressure and appreciable mole fraction of fuel and air, the dependecies of which are outlined in the range of validity of the theory, Section 3.4.

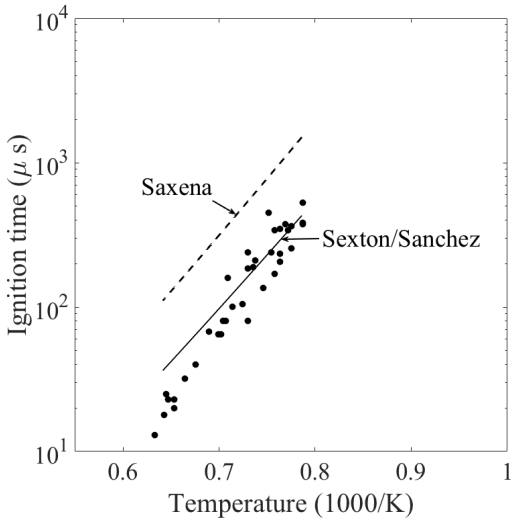

Figure 6: Comparison of experimental shock tube data [7] to analytic expressions for homogenous autoignition time of n-heptane.

N-heptane ignition times show perhaps the best agreement of the fuels tested (Figure 6), mainly a result of the appreciable mole fraction of the fuel in the mixture. A range of pressures up to 4 bar were tested; much higher than this, and fuel and third body concentrations increase to a level that further underpredicts the ignition time through the term Ψ^2, as in the case for n-butane combustion.

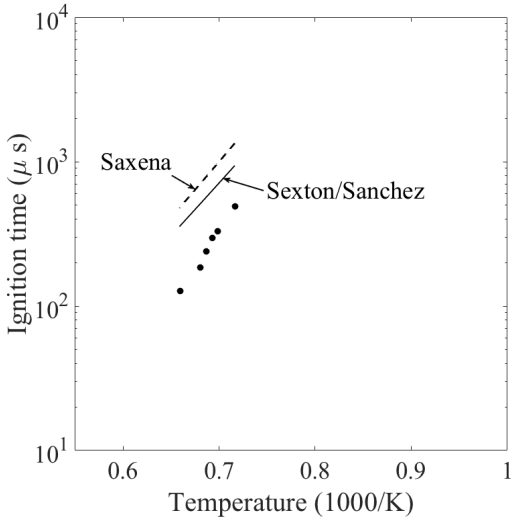

Figure 7: Comparison of experimental shock tube data [8] to analytic expressions for homogenous autoignition time of n-decane.

Low fuel concentrations also plagued the tests for n-decane (Figure 7), though the thermal runaway expression shows better agreement than for propane and Saxena's fuel depletion expression, since decane molecules are larger and break down into more larger hydrocarbon radicals. Higher heat release from larger molecules decomposing contributes significantly more to the temperature rise than smaller molecules such as propane or n-butane. Values of $\mathrm{q_I}$ and $\mathrm{q_{II}}$ for n-decane are up to 3.5 times higher than those of propane, leading to a greater influence of $\mathrm{q_I}$ and $\mathrm{q_{II}}$, even at small fuel fractions.

3.4 Range of Validity of the Updated Ignition Time Expression

Peters [2] makes clear the reduced chemical kinetic mechanism used here is limited to temperatures in the "high temperature regime," that is, temperatures above the crossover temperature ($\mathrm{T} > \mathrm{T}^*$, or $1000/\mathrm{K} \lesssim 1$). Ignition times in this temperature range exhibit an approximate linear dependence on initial mixture temperature $\mathrm{T_0}$, which allows for one simple ignition time equation, as was derived in 2.2, rather than a group of equations describing multiple stages of ignition. This temperature range is also the location in which our assumptions regarding steady state radicals hold true.

Influence of heat addition in the updated ignition time expression relies on the concentration of fuel in the mixture relative to other constituents. The number of moles of fuel in the overall mixture dictates how much energy will be released through decomposition of intermediate radicals into CO and $\mathrm{H_2O}$. Therefore, if the fuel-air portion of the mixture makes up an appreciable portion of the mixture($\sim 30\%$ fuel + air), the thermal runaway ignition time expression will yield significant improvements over the fuel depletion expression. If the fuel's mole fraction is much less than 2%, the heat addition has diminishing influence on temperature rise of the reaction, therefore does not predict ignition times significantly better than Saxena's expression, as was the case with propane and n-decane in Figures 3 and 7.

4 Supersonic Mixing Layer

Mixing of fuel and air streams in scramjet engines may be described as a supersonic-subsonic free shear layer. By nondimensionalizing the properties of each constituent with the properties of the inlet air stream, the solution becomes self similar, and can be integrated numerically to find the evolution of temperature, mass fraction of fuel and air, stream- and spanwise velocities, and thermodynamic and transport properties of the fuel-air mixture.

Very high shear forces act on the mixing layer due to the large velocity difference between the fuel and air streams. It is found in the energy equation, for typical supersonic flight velocities and altitudes, the viscous dissipation between the two streams causes a $30 - 40\%$ temperature rise in the shear layer. This indicates the maximum temperature of the mixing layer is not necessarily at the hotter of the two streams, but exists somewhere in the middle of the interaction of the two constituents. This nonmonotonic distribution gives way to unusual variations in the density and binary diffusion coefficient.

The chemically frozen mixing layer is useful in finding the evolution of temperature and mass fractions in supersonic combustion chambers, which are computed here. These values are necessary to find ignition times in Section 3.2, which, in future work, may be used as a perturbation to the mixing layer temperature distribution to find induction lengths for scramjet engines.

Similar problems have been addressed a number of times for different fuels and assumptions. Im *et al.* [9] solved the mixing and ignition problem for a nondescript hydrocarbon-air mixture, assuming constant properties (constant ρ, $\mathrm{C_p}$, and μ, so that Le=Pr=1), and found temperature rises associated with thermal runaway once combustion had been initiated within the mixing layer. Fernández-Tarrazo *et al.* [10] have solved a similar problem for hydrogen mixing layers, while addressing the combustion at initial mixture temperatures below crossover, where they accounted for changes in thermodynamic and transport properties similar to the present work. In 1987, Jackson and Hussaini [11] conducted an asymptotic analysis of two supersonic reacting streams mixing to the point of ignition, and found ignition distances for different values of the activation energy β.

This work aims to investigate the self similar temperature and fuel distributions of different hydrocarbons mixing with an air stream at Mach numbers from 1 to 10. The same fuels are explored here as in Section 3, and the conservation equations are integrated numerically for conditions surrounding supersonic and hypersonic flight.

4.1 Formulation of the Mixing Layer Problem

As mixing layer widths scale as $\delta \sim \sqrt{\mathrm{x}\mu_1/\mathrm{u}_1\rho_1} \sim 1\mathrm{E}-4$ m, the assumption that the shear layer is two dimensional holds well for most of the domain of interest (where μ_1, u_1, and ρ_1 denote properties of the supersonic air stream at the inlet). Due to the supersonic velocities found in scramjet engines, the mixing layer is slender, and the chemically frozen problem sees negligible changes in pressure. A more detailed analysis may show that ignition causes instabilities and pressure waves in the combustion chamber as noted by Huete *et al.* [1], but is far beyond the scope of this study.

External heating and cooling effects are also minimal and therefore neglected in this analysis, influences of which have been investigated in work by Im, Bechtold, and Law [16] . The only heating of the air above ambient temperature may be by shock heating experienced when entering the supersonic inlet [1].

The two dimensional, steady state, slender conservation equations are:

$$\frac{\partial}{\partial \mathrm{x}}(\rho \mathrm{u}) + \frac{\partial}{\partial \mathrm{z}}(\rho \mathrm{v}) = 0 \tag{45}$$

$$\rho \mathrm{u}\frac{\partial \mathrm{u}}{\partial \mathrm{x}} + \rho \mathrm{v}\frac{\partial \mathrm{u}}{\partial \mathrm{z}} = \frac{\partial}{\partial \mathrm{z}}(\mu \frac{\partial \mathrm{u}}{\partial \mathrm{z}}) \tag{46}$$

$$\rho \mathrm{u}\frac{\partial \mathrm{Y}}{\partial \mathrm{x}} + \rho \mathrm{v}\frac{\partial \mathrm{Y}}{\partial \mathrm{z}} = \frac{\partial}{\partial \mathrm{z}}(\rho \mathrm{D}\frac{\partial \mathrm{Y}}{\partial \mathrm{z}}) \tag{47}$$

$$\begin{aligned}\rho \mathrm{C_p}(\mathrm{u}\frac{\partial \mathrm{T}}{\partial \mathrm{x}} + \mathrm{v}\frac{\partial \mathrm{T}}{\partial \mathrm{z}}) =& \frac{\partial}{\partial \mathrm{z}}(\mathrm{k}\frac{\partial \mathrm{T}}{\partial \mathrm{z}}) + \mu(\frac{\partial \mathrm{u}}{\partial \mathrm{z}})^2 \\ &+ \rho D(\mathrm{C_{p_1}} - \mathrm{C_{p_2}})\frac{\partial \mathrm{Y}}{\partial \mathrm{z}}\frac{\partial \mathrm{T}}{\partial \mathrm{z}}\end{aligned} \tag{48}$$

where ρ is density, u and v are stream- and spanwise velocities, μ is the dynamic viscosity, Y is

the mass fraction of air, D is the diffusion coefficient of air into fuel, $\mathrm{C_p}$ is the mass specific heat capacity, T is temperature, and k is thermal conductivity. Equations 45-48 may be written in terms of the self similar coordinate η, by introducing the following variables, similar to the analyses by Im [9] and Fernández-Tarrazo [10]:

$$\eta = \mathrm{z}\sqrt{\frac{\mathrm{u}_1'\rho_1'}{\mathrm{x}\mu_1'}} \tag{49}$$

$$\mathrm{V} = \mathrm{v}\sqrt{\frac{\rho_1'\mathrm{x}}{\mu_1'\mathrm{u}_1'}} \tag{50}$$

All other properties are scaled with the properties of the supersonic air stream at x=0, and are dimensionless unless denoted by $'$ ($\mathrm{U} = \mathrm{u}'/\mathrm{u}_1', \mathrm{T} = \mathrm{T}'/\mathrm{T}_1'$, etc.) Substituting Equations 49-50 into 45-48 and reorganizing, finding the solution of the chemically frozen supersonic mixing layer becomes a problem of integrating the system of four coupled nonlinear partial differential equations:

$$-\frac{\eta}{2}\frac{\partial}{\partial\eta}(\rho\mathrm{U}) + \frac{\partial}{\partial\eta}(\rho\mathrm{V}) = 0 \tag{51}$$

$$\rho(\mathrm{V} - \frac{\eta}{2}\mathrm{U})\frac{\partial\mathrm{U}}{\partial\eta} = \frac{\partial}{\partial\eta}(\mu\frac{\partial\mathrm{U}}{\partial\eta}) \tag{52}$$

$$\rho(\mathrm{V} - \frac{\eta}{2}\mathrm{U})\frac{\partial\mathrm{Y}}{\partial\eta} = \frac{\partial}{\partial\eta}(\frac{\rho\mathrm{D}}{\mathrm{Sc}}\frac{\partial\mathrm{Y}}{\partial\eta}) \tag{53}$$

$$\rho\mathrm{C_p}(\mathrm{V} - \frac{\eta}{2}\mathrm{U})\frac{\partial\mathrm{T}}{\partial\eta} = \frac{\partial}{\partial\eta}(\frac{\mathrm{k}}{\mathrm{Pr}}\frac{\partial\mathrm{T}}{\partial\eta}) + (\gamma-1)\mathrm{M}_1^2\mu(\frac{\partial\mathrm{U}}{\partial\eta})^2 \tag{54}$$

$$+ \frac{\rho\mathrm{D}}{\mathrm{Sc}}\frac{\partial\mathrm{Y}}{\partial\eta}\frac{\partial\mathrm{T}}{\partial\eta}(\mathrm{C_{p1}} - \mathrm{C_{p2}}) \tag{55}$$

where $\mathrm{Pr} = \mu_1'\mathrm{C_{p_1}}'/\mathrm{k}_1'$ is the Prandtl number, and $\mathrm{Sc} = \mu_1'/\rho_1'\mathrm{D}_1'$ is the Schmidt number of the air stream at the inlet. Variations in thermodynamic and transport properties are computed using relationships from Reid, Prausnitz, and Poling [17]. Most interesting of these are density and the binary diffusion coefficient, which exhibit a minimum and maximum inside the mixing layer (Figures 9-13).

Prandtl and Schmidt numbers arise from nondimensionalizing the problem by properties

found in the air stream. The term $(\gamma - 1)\mathrm{M}^2$ emerges as a result of substituting $\mathrm{U} = \mathrm{u}'/\mathrm{u}_1'$ into the squared term $(\partial \mathrm{u}'/\partial \mathrm{z})^2$, giving way to $\mathrm{u}_1'^2 = \mathrm{M}^2\sqrt{\gamma \mathrm{R}\mathrm{T}_1'}^2$, where $\mathrm{R} = \mathrm{C}_\mathrm{p}' - \mathrm{C}_\mathrm{v}'$. Dividing by ${\mathrm{C}_\mathrm{p}}_1'$ and T_1' reduces $\gamma(\mathrm{C}_\mathrm{p}' - \mathrm{C}_\mathrm{v}')\mathrm{T}_1'$ to $(\mathrm{C}_\mathrm{p}'/\mathrm{C}_\mathrm{v}' - \mathrm{C}_\mathrm{v}'/\mathrm{C}_\mathrm{v}') = (\gamma - 1)$.

Equation 51 is a first order nonlinear differential equation, thus requires one boundary condition for V. Equations 52-55 are all second order in η, requiring one boundary condition at each side of the domain. The initial conditions for the solutions of streamwise velocity U and mass fraction Y are estimated using an error function, the spanwise velocity distribution V estimated as parabolic, and the temperature distribution was initially a flat line from either side of the domain so that $\mathrm{T}(-\infty, \infty) = 1$. Equations 51-55 were integrated using the Chebfun toolbox [18] in MATLAB over $\eta = -\infty \rightarrow \infty$ with boundary conditions $\mathrm{T}(-\infty) = \mathrm{T}(\infty) = 1$, $\mathrm{U}(-\infty) = \mathrm{U}_1$, $\mathrm{U}(\infty) = 1$, $\mathrm{Y}(-\infty) = 0$, $\mathrm{Y}(\infty) = 1$, and $\mathrm{V}(0) = 0$.

4.2 Results of the Numerical Integration

The shape of the temperature distribution is mainly influenced by the viscous dissipation term $\Omega = (\gamma - 1)\mathrm{M}^2$, and the difference in temperatures of the air and fuel streams $\mathrm{T}_\mathrm{a}/\mathrm{T}_\mathrm{f}$, if one exists. The viscous dissipation term Ω causes a peak in the middle of the temperature profile, while the temperature difference $\mathrm{T}_\mathrm{a}/\mathrm{T}_\mathrm{f}$ affects the overall slope of the temperature distribution.

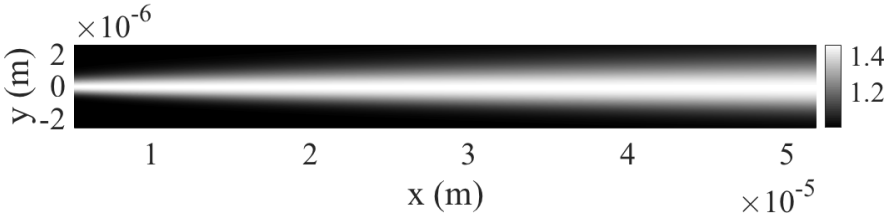

Figure 8: Two dimensional temperature distribution for $\Omega = 10$ ($\mathrm{M} \approx 5$) and $\mathrm{T}_\mathrm{a}/\mathrm{T}_\mathrm{f} = 1$.

Figures 9-13 show temperature, fuel mass fraction, stream- and spanwise velocities U and V, as well as thermodynamic and transport properties of the mixing layer for propane, butane, pentane, heptane, and decane. These results were integrated for $\Omega = 10$, which corresponds to a chamber mach number of $\mathrm{M} \approx 5$. There are clear differences in properties of each fuel,

such as heavier hydrocarbon fuels demonstrating larger heat capacities and smaller viscosities. Computation of these properties per [17] are demonstrated in Section 4.3.

There is a nonzero spanwise velocity V over most of η, save the middle near where $\eta = 0$. Spanwise velocity V is strongly affected by the density changes near $\eta = 0$, a result of the conservation of momentum. U velocity and fuel mass fraction $\mathrm{Y_f}$ follow a rather unremarkable error function and complimentary error function, as expected given the general solution to their second order partial differential equations (note: Y in Equations 51-55 is mass fraction of air. Here, $\mathrm{Y_f} = (1 - \mathrm{Y_a})$.). Specific heat capacity $\mathrm{C_p}$ falls approximately with $\mathrm{Y_f}$, but also has a slight influence from T, causing the slope to lessen near $\eta = 0$. Thermal conductivity exhibits similar behavior to $\mathrm{C_p}$, but increases as the air stream dominates, instead of decreasing. Finally, density decreases with mass fraction, as the fuels here are all heavier than oxygen. However, density does see a noticeable effect from the temperature peak near $\eta = 0$, that is, it decreases below the density of the air stream. This behavior highlights the requirement to adjust thermodynamic and transport properties as they change, as simpler relations based on either mass fraction or temperature alone would not demonstrate these artifacts.

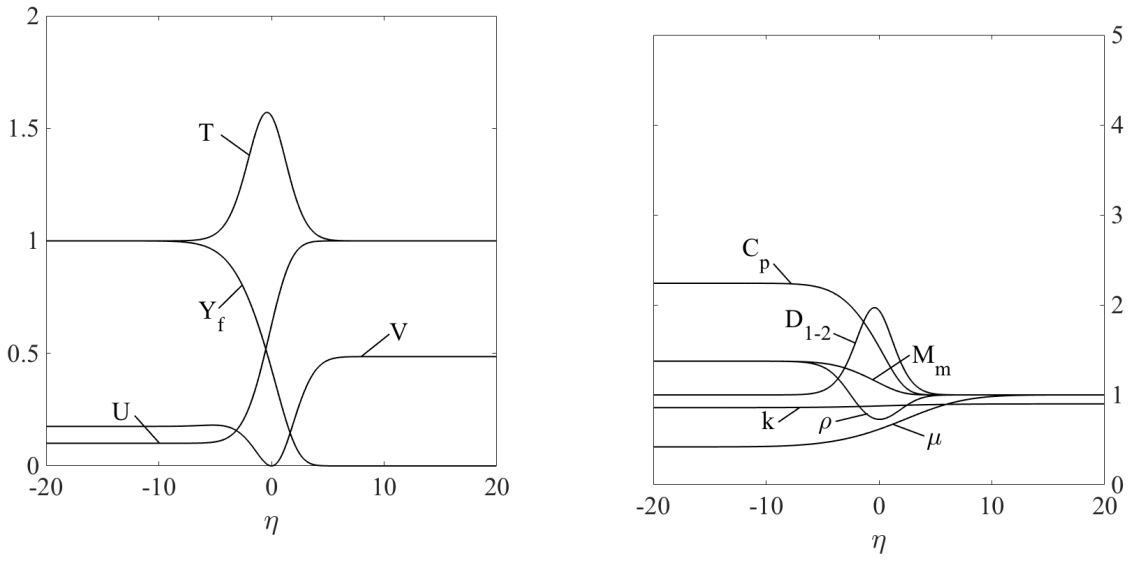

Figure 9: Temperature, fuel mass fraction, stream- and spanwise velocities, and thermodynamic and transport properties of propane-oxygen mixing layer.

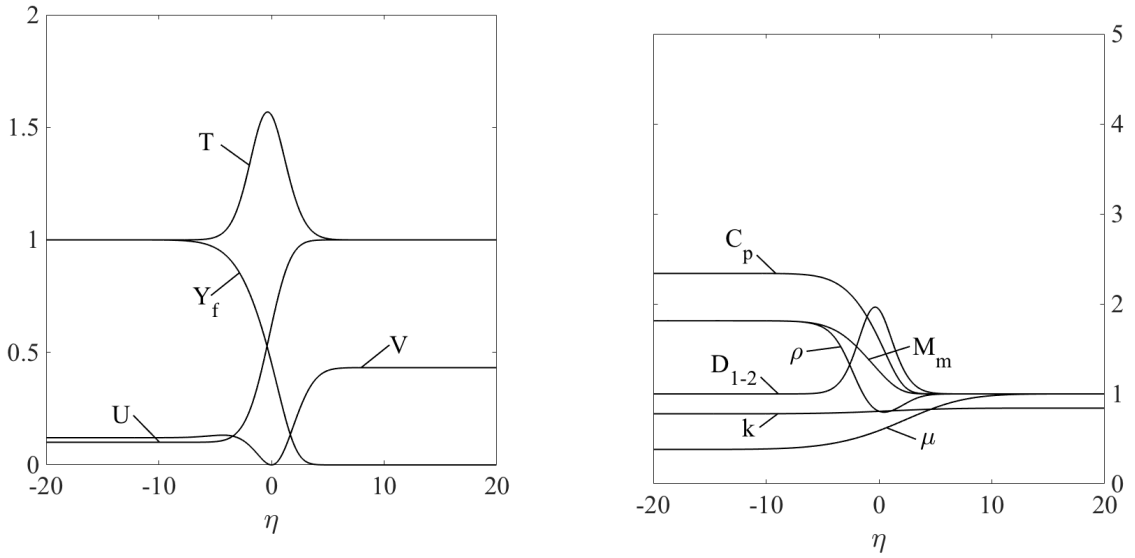

Figure 10: Temperature, fuel mass fraction, stream- and spanwise velocities, and thermodynamic and transport properties of butane-oxygen mixing layer.

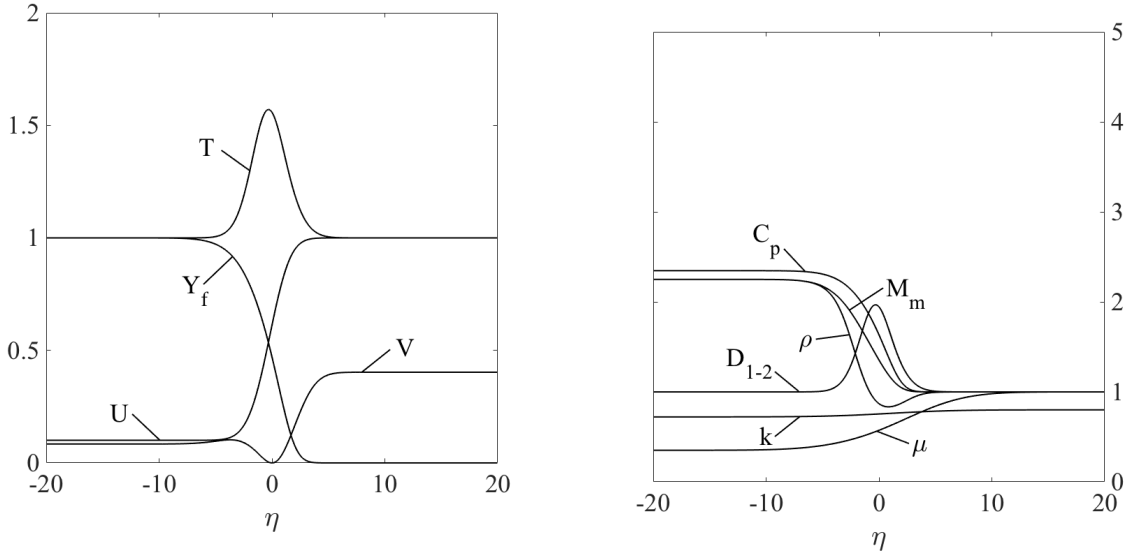

Figure 11: Temperature, fuel mass fraction, stream- and spanwise velocities, and thermodynamic and transport properties of pentane-oxygen mixing layer.

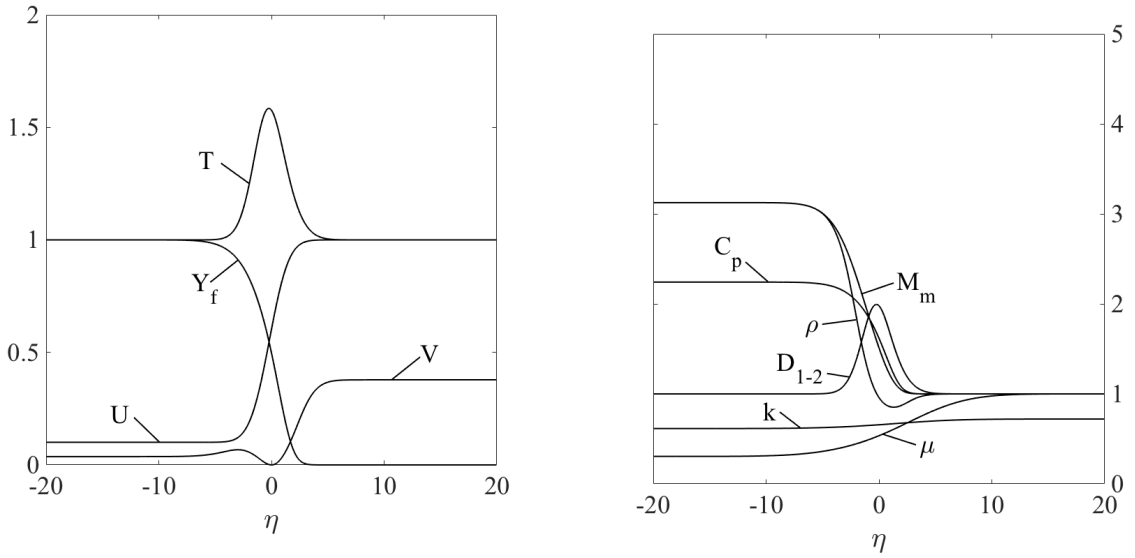

Figure 12: Temperature, fuel mass fraction, stream- and spanwise velocities, and thermodynamic and transport properties of heptane-oxygen mixing layer.

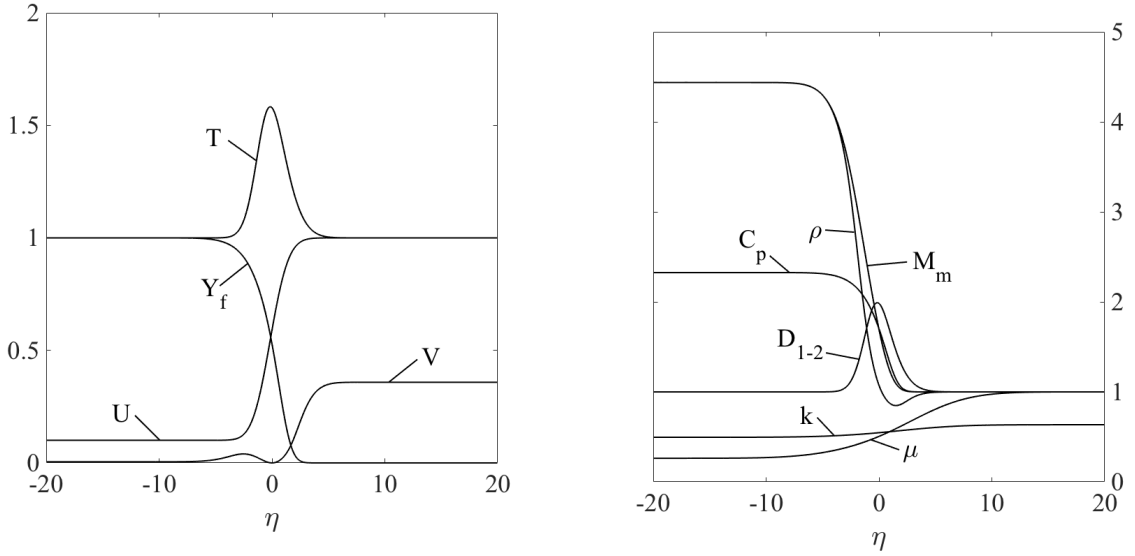

Figure 13: Temperature, fuel mass fraction, stream- and spanwise velocities, and thermodynamic and transport properties of decane-oxygen mixing layer.

4.2.1 Temperature Rise by Viscous Heating

In free shear layers with velocity differences between two streams of order $\mathrm{M} = 1$, heating by viscous dissipation becomes an appreciable contribution of heating in the stream. Influences of this stem from what we will refer to as the viscous dissipation term $\Omega = (\gamma - 1)\mathrm{M}^2$. Results of the temperature distribution are plotted for values of $\Omega = 1$ to $\Omega = 25$ in Figure 14. As expected, raising the velocity of the supersonic air stream relative to the subsonic fuel stream increases viscous heating effects, and the temperature rises near $\eta = 0$. This result is useful in the design of scramjet engines, as it allows for viscous heating to initiate the combustion reaction inside a supersonic combustion chamber. However, these simulations only demonstrate the temperature rise for the chemically frozen mixing layer, numerical and analytic analyses of the non-frozen solution are a task for future work.

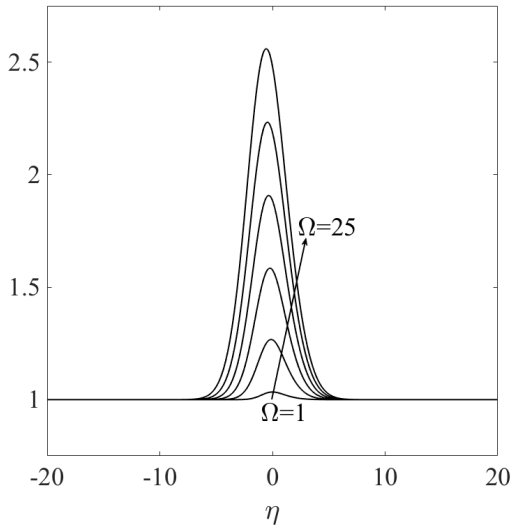

Figure 14: Effect of increasing viscous dissipation $\Omega = (\gamma - 1)\mathrm{M}^2$. $\Omega = 1$ corresponds to $\mathrm{M} \approx 1.5$, and $\Omega = 25$ to $\mathrm{M} \approx 10$.

4.2.2 Effect of the Boundary Temperature Difference $\mathrm{T_a}/\mathrm{T_f}$

Changing the value of fuel temperature with respect to that of air changes the overall profile, creating a sort of step in temperature across the mixing layer. There is almost no variation in temperature of the fuel or air stream until $\eta \approx \pm 4$, roughly where the distribution for $\mathrm{T_a}/\mathrm{T_f} = 1$ exhibits a change in slope regardless of temperature difference. This means special attention need not be paid to supersonic inlet design with higher air stream temperatures, as the nonreacting stage of fuel will see similar temperatures for all air temperatures. However, Boivin *et al.* [14] show this temperature rise occurs much further from $\eta = 0$ once combustion is initiated.

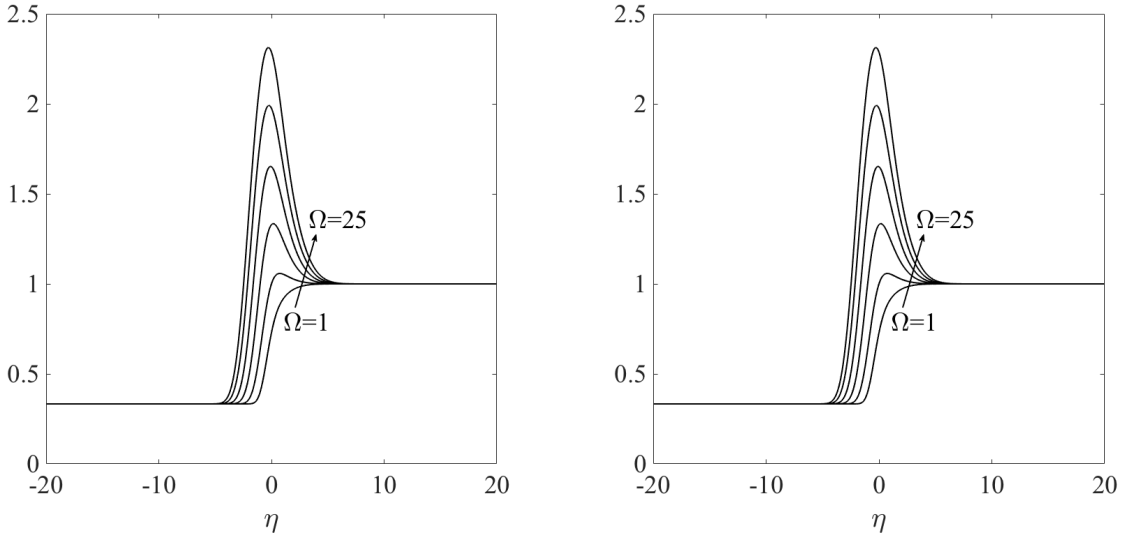

Figure 15: Temperature profiles for $\Omega = 25$, with $\mathrm{T_a}/\mathrm{T_f} = 3$ (left) and $\mathrm{T_a}/\mathrm{T_f} = 2$ (right). Peak temperatures are 2.313 and 2.475, compared to 2.559 for $\mathrm{T_a}/\mathrm{T_f} = 1$ (Figure 14).

Figure 16 shows the peaks in temperature for $\Omega = 10$ of simulations for variation in $\mathrm{T_a}/\mathrm{T_f}$. These peaks exhibit a clear dependence on the fuel stream temperature $\mathrm{T_f}$, so that when fuel stream temperature is lower, the peak is lower as well. The secondary effect, however, is that lower temperatures produce lower viscosities in the stream. Viscous heating is result of the product $\Omega\mu$, so with a lower viscosity value, one should expect to see less viscous heating, as well.

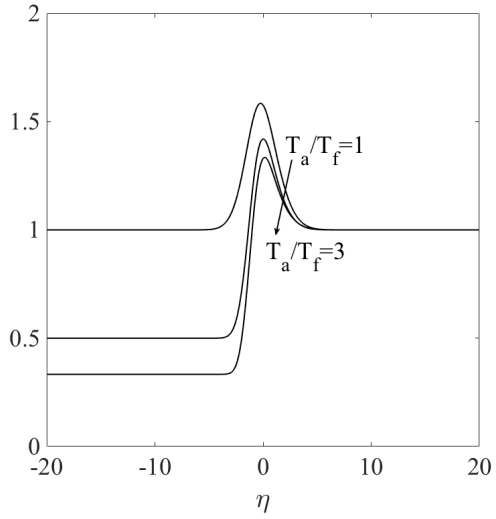

Figure 16: Comparison of heptane-oxygen temperature distribution peaks for $\Omega = 10$ and $\mathrm{T_a/T_f} = 1$, 2, and 3.

4.3 Computation of Thermodynamic and Transport Properties

Equations 51-55 involve various thermodynamic and transport properties of the air and fuel streams. These properties are primarily dependent on mass fraction and temperature, the variations of which are shown in Figures 9-13.

4.3.1 Thermodynamic properties

Density of a binary gas mixture is dependent of the molecular weight of the two gases, mass fraction of those two gases in the mixing layer, and the temperature of the mixing layer at that point. These properties may be related with an equation of state, which is normalized with the properties of the air stream. Taking the equation of state for the mixture and for the air stream, with $'$ denoting dimensional values:

$$\mathrm{P}' = \rho' \frac{\mathrm{R}}{\mathrm{M}'} \mathrm{T}' \tag{56}$$

$$\mathrm{P}'_{\mathrm{a}} = \rho'_{\mathrm{a}} \frac{\mathrm{R}}{\mathrm{M}'_{\mathrm{a}}} \mathrm{T}'_{\mathrm{a}} \tag{57}$$

Assuming no pressure gradient across the mixing layer, and dividing Equation 56 by Equation 57,

we have:

$$1 = \frac{\rho'}{\rho'_{\mathrm{a}}} \frac{\mathrm{M}'_{\mathrm{a}}}{\mathrm{M}'} \frac{\mathrm{T}'}{\mathrm{T}'_{\mathrm{a}}} = \rho \mathrm{T} \frac{\mathrm{M}'_{\mathrm{a}}}{\mathrm{M}'} \tag{58}$$

Separating $\rho\mathrm{T}$ and $\mathrm{M}'_{\mathrm{a}}/\mathrm{M}'$ and expanding for the mean molecular mass M', we have an expression for density relating mass fraction $\mathrm{Y_a}$, T, and $\mathrm{M_f} = \mathrm{M}'_{\mathrm{f}}/\mathrm{M_a}$:

$$\rho = \frac{1}{\mathrm{T}(\mathrm{Y_a} + (1 - \mathrm{Y_a})\mathrm{M_f^{-1}})} \tag{59}$$

Thermal conductivity of a mixture can be estimated by use of the Wassiljewa equation [17], along with the Mason and Saxena approximation for the function $\mathrm{A_{ij}}$:

$$\mathrm{k_m} = \sum_{\mathrm{i}=1}^{\mathrm{n}} \frac{\mathrm{x_i k_i}}{\sum_{\mathrm{j}=1}^{\mathrm{n}} \mathrm{x_j A_{ij}}} \tag{60}$$

where $\mathrm{x_i}$ is the mole fraction of each species in the mixture. The Mason And Saxena approximation for $\mathrm{A_{ij}}$ suggests:

$$\mathrm{A_{ij}} = \frac{\epsilon(1 + (\mathrm{k_{tr_i}}/\mathrm{k_{tr_j}})^{1/2}(\mathrm{M_i}/\mathrm{M_j})^{1/4})^2}{(8(1 + \mathrm{M_i}/\mathrm{M_j}))^{1/2}} \tag{61}$$

where $\mathrm{k_{tr_i}}$ is the monatomic thermal conductivity, and ϵ is a constant of order unity, and $\mathrm{A_{ii}} = 1$. Reid *et al.* [17] recommend the Mason and Saxena approach to compute $\mathrm{A_{ij}}$ for nonpolar gas mixtures, and suggest errors will typically be less than 5%. The ratio $\mathrm{k_{tr_i}}/\mathrm{k_{tr_j}}$ may be found by the Roy-Thodos estimation technique:

$$\Gamma_{\mathrm{i}} = 210(\frac{\mathrm{T_c M^3}}{\mathrm{P_c^4}})^{1/6} \tag{62}$$

$$\frac{\mathrm{k_{tr_i}}}{\mathrm{k_{tr_j}}} = \frac{\Gamma_{\mathrm{j}}(\exp(0.0464\mathrm{T_{r_i}}) - \exp(-0.2412\mathrm{T_{r_i}}))}{\Gamma_{\mathrm{i}}(\exp(0.0464\mathrm{T_{r_j}}) - \exp(-0.2412\mathrm{T_{r_j}}))} \tag{63}$$

where $\mathrm{P_c}$, $\mathrm{T_c}$, and $\mathrm{T_r}$ are the critical and reduced values of pressure and temperature. This method

is useful in that it does not require experimental data for thermal conductivities, but can estimate them from critical thermodynamic properties of each constituent. The air stream's conductivity does need to be known to calculate Prandtl number. The Roy Thodos technique defines a reduced thermal conductivity composed of translational and interchange energy (rotational, vibrational, etc.) terms:

$$\mathrm{k_r\Gamma} = (\mathrm{k\Gamma})_{\mathrm{tr}} + (\mathrm{k\Gamma})_{\mathrm{int}} \tag{64}$$

$$(\mathrm{k\Gamma})_{\mathrm{tr}} = 8.757(\exp(0.0464\mathrm{T_r})\exp(-0.2412\mathrm{T_r})) \tag{65}$$

$$(\mathrm{k\Gamma})_{\mathrm{int}} = \mathrm{Cf}(\mathrm{T_r}) \tag{66}$$

$$\mathrm{f}(\mathrm{T_r}) = -0.152\mathrm{T_r} + 1.191\mathrm{T_r^2} - 0.039\mathrm{T_r^3} \tag{67}$$

where Equation 67 is valid for saturated hydrocarbons, and C is found based on the base group and number and type of methyl substitutions of the hydrocarbon fuel. Thermal conductivity k is found by dividing Equation 64 by Equation 62 solved for air.

Mass specific heat capacity $\mathrm{C_p}$ is estimated with a simple mass fraction weighted average, normalized by the specific heat of air ($\mathrm{Y_i}$ is the mass fraction of constituent i):

$$\mathrm{C_p} = \frac{\mathrm{C'_{p_a}Y_a} + \mathrm{C'_{p_f}Y_f}}{\mathrm{C'_{p_a}}} \tag{68}$$

All thermodynamic properties take on the fuel's dimensionless value at the fuel boundary and converge on $\rho = \mathrm{k} = \mathrm{C_p} = 1$ at the air boundary (Figures 9-13).

4.3.2 Transport properties

A corresponding states method was employed to find the binary mixture viscosity, per Lucas rules for mixture properties [17]:

$$\mathrm{T_{c_m}} = \sum_{\mathrm{i}} \mathrm{x_i T_{c_i}} \tag{69}$$

$$\mathrm{P_{c_m}} = \mathrm{RT_{c_m}} \frac{\sum_\mathrm{i} \mathrm{x_i Z_{c_i}}}{\sum_\mathrm{i} \mathrm{x_i V_{c_i}}} \tag{70}$$

$$\mathrm{M_m} = \sum_\mathrm{i} \mathrm{x_i M_i} \tag{71}$$

These mixture properties were applied:

$$\xi = 0.176 \left(\frac{\mathrm{T_c}}{\mathrm{M^3 P_c^4}}\right)^{1/6} \tag{72}$$

$$\begin{aligned} \mu\xi =& (0.807 \mathrm{T_r^{0.618}} - 0.357 \exp(-0.449 \mathrm{T_r}) \\ &+ 0.340 \exp(-4.058 T_r) + 0.018) \mathrm{F_P^o F_Q^o} \end{aligned} \tag{73}$$

where $\mathrm{F_P^o}$ and $\mathrm{F_Q^o}$ account for polarity and quantum effects, both negligible for gases in this analysis. Viscosity is found by dividing Equation 73 by Equation 72.

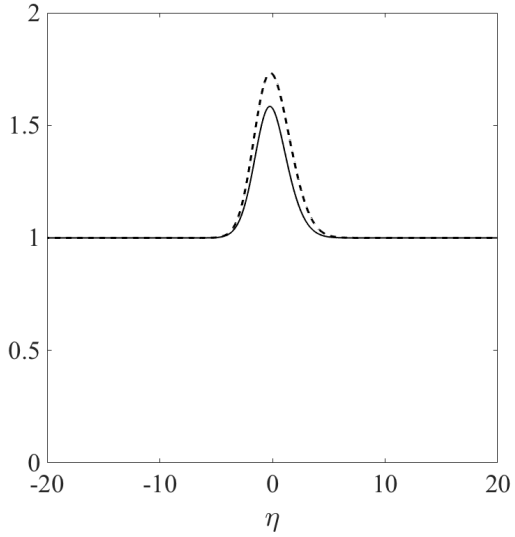

Figure 17: Heptane-air temperature profile for mixing layer with variable viscosity (solid) and $\mu = 1$ (dashed). Maximum error is 25% of the temperature rise.

To demonstrate the necessity of computing the variation in transport properties, Figure 17 shows the temperature distribution for $\Omega = 10$ and $\mathrm{T_a/T_f} = 1$, taking into account variation of viscosity vs. the temperature distribution for $\mu = 1$. For a heptane-air mixture, the viscosity varies by four times across the mixing layer The simplification of constant viscosity overpredicts the

temperature rise by roughly 25%.

Calculation of the dimensionless binary diffusion coefficient was reduced to a simple temperature dependence, which rises from nondimensionalizing Equation 78 by itself to find the inlet diffusion coefficient:

$$\mathrm{D} = \mathrm{T}^{1.5} \tag{74}$$

Because the Schmidt number depends on the diffusion coefficient D, one must find the diffusion coefficient at the temperature of the air inlet. The Lennard-Jones 12-6 potential [17] was used to compute the value of D at the temperature of the hot air stream:

$$\epsilon_{\mathrm{AB}} = (\epsilon_{\mathrm{A}}\epsilon_{\mathrm{B}})^{1/2} \tag{75}$$

$$\sigma_{\mathrm{AB}} = \frac{\sigma_{\mathrm{A}} + \sigma_{\mathrm{B}}}{2} \tag{76}$$

$$\Omega_{\mathrm{D}} = \frac{\mathrm{A}}{(\mathrm{T}^*)^{\mathrm{B}}} + \frac{\mathrm{C}}{\exp(\mathrm{DT}^*)} + \frac{\mathrm{E}}{\exp(\mathrm{FT}^*)} + \frac{\mathrm{G}}{\exp(\mathrm{HT}^*)} \tag{77}$$

$$\mathrm{D}_{\mathrm{AB}} = \frac{0.00266\mathrm{T}^{3/2}}{\mathrm{PM}_{\mathrm{AB}}^{1/2}\sigma_{\mathrm{AB}}^2\Omega_{\mathrm{D}}} \tag{78}$$

D's dependence on temperature is clear in Figures 9-13, with peaks near $\eta = 0$, a direct result of the rise in temperature. Transport properties, similar to thermodynamic properties, converge on $\mu = \mathrm{D} = 1$ near the air boundary.

4.3.3 Nondimensional Numbers

The Prandtl number, Schmidt number, and Mach number (Pr, Sc, and M) introduce the relative influence of each constituent's transport and thermodynamic properties to the conservation equations, and relate the level of authority of each property over the solution. They are calculated

with properties of the inlet air stream as follows:

$$\mathrm{Pr} = \frac{\mu' \mathrm{C}'_{\mathrm{p}}}{\mathrm{k}'} \tag{79}$$

$$\mathrm{Sc} = \frac{\mu'}{\rho' \mathrm{D}'} \tag{80}$$

$$\mathrm{M} = \frac{\mathrm{u}'}{\sqrt{\gamma \mathrm{R} \mathrm{T}'}} \tag{81}$$

5 Conclusion

Use of an improved analytic expression for hydrocarbon ignition times in conjunction with detailed mixing layer solutions will permit future calculation of induction lengths in scramjet engines. These lengths may be found analytically or numerically, for both of which the groundwork was laid in the present work.

Computation of hydrocarbon autoignition times with previously derived analytic expressions [3] and the updated chemical kinetic mechanism [4] showed the expression falls out of agreement with experimental shock tube data [5]- [8]. A new version of this expression was proposed here, using thermal runaway as the criterion for ignition rather than fuel depletion. The new expression includes heats of reaction from decomposition of the parent fuel into its final products. This decomposition is exothermic, releasing heat and reducing the time to thermal runaway. This decrease in ignition time resulted in improvement of estimates for five n-alkanes in comparison with the previous expression and experimental data.

Numerical integration of the conservation equations in a supersonic mixing layer revealed a temperature peak in the layer near $\eta = 0$. This peak is a result of viscous heating, and as the velocity of the supersonic air stream is increased with respect to that of the fuel stream, the so called viscous heating term Ω grows, increasing the magnitude of the temperature peak. Investigation of thermodynamic and transport properties showed their variation has a great influence on the final temperature distribution. Neglecting these properties may produce errors in the temperature rise of 25% or higher.

Logical continuation of this work include numerical investigation of combining the mass and energy conservation equations from Section 3.2 with those of Section 4.1, and an analytic perturbation analysis of the mixing layer temperature profile perturbed by the activation energy β from Section 3.2.

References

[1] César Huete, Antonio Sánchez, and Javier Williams, Forman Urzay. Theory of weak-shock interactions with transonic mixing layers. *25th ICDERS*, August 2015.

[2] N. Peters, G. Paczko, R. Seiser, and K. Seshadri. Temperature cross-over and non-thermal runaway at two-stage ignition of n-heptane. *Combustion and Flame*, 128(1):38–59, 2002.

[3] P. Saxena, N. Peters, and F. A. Williams. An analytical approximation for high-temperature autoignition times of higher alkanes. *Combustion and Flame*, 149(1):79–90, 2007.

[4] Antonio L. Sánchez and Forman A. Williams. Corrigendum to recent advances in understanding of flammability characteristics of hydrogen. *Progress in Energy and Combustion Science*, 54(Supplement C):93–94, 2016.

[5] Jeffrey A. Gray and Charles K. Westbrook. High-temperature ignition of propane with mtbe as an additive: Shock tube experiments and modeling. *International Journal of Chemical Kinetics*, 26(7):757–770, 1994.

[6] Alexander Burcat, Karl Scheller, and Assa Lifshitz. Shock-tube investigation of comparative ignition delay times for c1-c5 alkanes. *Combustion and Flame*, 16(1):29–33, 1971.

[7] D.J. Vermeer, J.W. Meyer, and A.K. Oppenheim. Auto-ignition of hydrocarbons behind reflected shock waves. *Combustion and Flame*, 18(3):327–336, 1972.

[8] D. C. Horning, D. F. Davidson, and R. K. Hanson. Study of the high-temperature autoignition of n-alkane/o/ar mixtures. *Journal of Propulsion and Power*, 18(2):363–371, Mar 2002.

[9] H. G. Im, B. H. Chao, J. K. Bechtold, and C. K. Law. Analysis of thermal ignition in the supersonic mixing layer. *AIAA Journal*, 32(2):341–349, Feb 1994.

[10] Eduardo Fernández-Tarrazo, Antonio L. Sánchez, and Forman A. Williams. Hydrogen-air mixing-layer ignition at temperatures below crossover. *Combustion and Flame*, 160(10):1981–1989, 2013.

[11] T. L. Jackson and M. Y. Hussaini. An asymptotic analysis of supersonic reacting mixing layers. *Combustion Science and Technology*, 57(4-6):129–140, 1988.

[12] The san diego mechanism. *http://web.eng.ucsd.edu/mae/groups/combustion/mechanism.html*, 2017.

[13] H. Pitsch. Entwicklung eines programmpaketes zur berechnung eindimensionaler flammen am beispiel einer gegenstromdiffusionsflamme. 1993.

[14] Pierre Boivin, Antonio L. Sánchez, and Forman A. Williams. Explicit analytic prediction for hydrogen-oxygen ignition times at temperatures below crossover. *Combustion and Flame*, 159(2):748–752, 2012.

[15] NIST chemistry webbook. *http://webbook.nist.gov/chemistry/*.

[16] H. G. Im, J. K. Bechtold, and C. K. Law. Analysis of thermal ignition in supersonic flat-plate boundary layers. *Journal of Fluid Mechanics*, 249:99–120, 1993.

[17] R.C. Reid, J.M. Prausnitz, and B.E. Poling. *The Properties of Gases and Liquids*. Chemical engineering series. McGraw-Hill, 1987.

[18] T. A. Driscoll, N. Hale, and L. N. Trefethen. Chebfun. 2014.